Innovative Modeling and Simulation of Reacting Flow with Complex Confined Boundaries

*Ki-Hong Kim, Jai-ick Yoh**
Department of mechanical and aerospace engineering, Seoul National University
Sinlim 9dong, Gwanakgu, Seoul, Korea
project4@snu.ac.kr, jjyoh@snu.ac.kr

Keywords: multi physics, reacting flow, energetic material, Eulerian methodology

Abstract

We present an innovative method of multi physics application involving energetic materials. Energetic materials are related to reacting flows in extreme environments such as fires and explosions. They typically involve high pressure, high temperature, strong shock waves and high strain rate deformation of metals. We use an Eulerian methodology to address these problems. Our approach is naturally free from large deformation of materials that make it suitable for high strain rate multi-material interacting problems. Furthermore we eliminate the possible interface smearing by using the level sets. We heave devised a new level set based tracking framework that can elegantly handle large gradients typically found in reacting gases and metals. We show several work-in-progress application of our integrated framework.

Introduction

High-speed impact of materials generates strong shock waves, high rate of deformations and generates hydrodynamic pressure that are often much greater than the deviatoric stresses of a shocked material. Then, variants of the standard Euler equations for compressible flow can be used to model the shocked condensed matter with its known structural properties. The dominant physical mechanisms satisfy the Euler equations to a first approximation, and the effects associated with deviatoric strength are in some sense a small correction.

The accurate and reliable simulation of the multi-material shock physics poses a great challenge to the wide range of hydrodynamic solvers developed until recently. Fedkiw et al. [1] proposed the ghost fluid concept which consists of both the level-set function and natural boundary conditions to model multi-gas interaction. The ghost fluid method has shown advantage over conventional sharp interface approach particularly for its simplicity in defining and imposing conditions at the boundaries of zero-level sets. Stewart et al. [2] carried out a detonation simulation of the energetic material where they showed a robust and efficient way of tracking detonation front by similar use of the level-sets explained in [1]. The elasto-plastic motion of metal was considered by Tran and Udaykumar [3]. The behavior of metal is modeled by the level-set function and the constitutive relations for ductile material. More recently, Liu et al. proposed a method of improving the original ghost fluid concept for tracking material interface [4]. They have reported the difficulty associated with the original method to when handling the strong shock impinging on a material's contact surface. Both the Rankine-Hugoniot jump conditions and the selective solutions of the Riemann problem are utilized in solving the shock-interface interaction.

In the past, hydrodynamic codes have been actively developed by the US Department of Energy (DOE) laboratories to model multi-dimensional, multi-material interactions with high-rates of deformations and high-frequency response of energetic materials in the presence of strong shock waves [5-7]. In particular, CTH developed at Sandia National Laboratories is an Eulerian method based hydrocode that has been successfully applied to a large variety of strong shock problems, which include hypervelocity impact and effects of detonating high explosives [5]. Both analytic and tabular equations of state (EOS) for solid, liquid, vapor, gas-liquid mixed phase and solid-liquid mixed phase have been implemented. A similar hydrocode, ALE3D of Lawrence Livermore National Laboratory is based on the Arbitrarily Lagrangian and Eulerian method that allows convective 'motion' of rapidly deforming Lagrangian grids [6]. PAGOSA of Los Alamos National Laboratory solves the conservation of mass, momentum, and energy equations across the `fixed' interface in two steps: A Lagrangian step where the cell distorts and follows the material motion, followed by a rezone step where the distorted cells are mapped back to the Eulerian mesh [7].

Typically these hydrocodes are first order in time and second order in space. Our high-resolution approach uses fourth-order convex ENO for the spatial discretization and third-order Runge-Kutta for time advancement. Our treatment of material interfaces uses level sets and is fairly simple and robust. Enforcement of jump conditions across the material interface is achieved by applying a ghost-point-populating technique to interpolate data into extended regions. The time advancement is based on the method of lines, and it enables multi-dimensional calculations without time splitting and allows efficient implementation of Runge-Kutta schemes at orders higher than two.

The physical models we use include an ideal equation of state (EOS) for inert compressible gas, ideal EOS reactive flow model for high-explosive (HE) that uses the reaction rate law, a Mie-Gruneisen EOS for inert solid, and an elasto-plastic model for

metal with isotropic linear hardening based on the Prandtl-Reuss model. In this paper, algorithmic discussions of Hydro-SCCM are presented. The paper is written with the aim that most reader would find the physical description of the method suitable for reproducing and building one's own hydrocode.

Physical description of a hyperbolic solver

The general conservation laws of multi-dimensional, multi-material physics can be written as

$$\frac{\partial U}{\partial t}+\frac{\partial F}{\partial x}+\frac{\partial G}{\partial y}=W(U) \tag{1}$$

where the variables represent a vector of conserved variables U, spatial fluxes in x and y-directions F and G, and a source, W. The discretized system of PDEs in (1) can be solved by independent steps of space and time integration. For our two-dimensional system, the x and y fluxes are treated with the third-order convex ENO scheme. Then the equation (1) is approximated by a system of ODEs in time that is solved by a fourth-order explicit and linearized implicit Runge-Kutta scheme [8].

Discretization in time

The third-order Runge-Kutta algorithm for time stepping is given by

$$U^{n+1}=U^{n}+\sum_{j=1}^{r}W_j k_j$$

$$k_i=\Delta t f(U^{n}+\sum_{j=1}^{i-1}b_{ij}k_j)+\Delta t W(U^{n}+\sum_{j=1}^{i}c_{ij}k_j)$$

$$(i=1,\ldots,r) \tag{2}$$

where the implicit RK coefficients c_{ij} are used for integrating the stiff chemical source term W(U) and the explicit RK coefficients b_{ij} are used for the convective and all other process modeling term f(U) in the governing equation (1).

Discretization in space

A brief discussion of the high order spatial descretization is given. Interested readers may find a full description from Ref. [9]. For a simple explanation, we consider a one-dimensional hyperbolic equation,

$$\frac{\partial u}{\partial t}+\frac{\partial f(u)}{\partial x}=0 \tag{3}$$

where the spatial derivative is replaced by a set of descretized fluxes

$$\frac{du}{dt}+\frac{1}{\Delta x}\left(\hat{f}_{j+1/2}-\hat{f}_{j-1/2}\right)=0 \tag{4}$$

The fluxes of a resulting ODE will determine the order of spatial accuracy. For a high-order ENO flux construction, a combination of upwind and downwind fluxes are suggested as

$$f^{+}_{j+1/2}(u)=\frac{1}{2}\left(f(u)+\alpha_{j+1/2}u\right),$$

$$f^{-}_{j+1/2}(u)=\frac{1}{2}\left(f(u)-\alpha_{j+1/2}u\right) \tag{5}$$

The variation in α would control the amount of viscosity or diffusion of the approximation. For the local Lax-Friedrichs fluxes as used in this work,

$$\alpha_{j+1/2}=\max_{\min(u_j,u_{j+1})\le u\le\max(u_j,u_{j+1})}\left|\frac{\partial f}{\partial u}\right| \tag{6}$$

where $\alpha_{j+1/2}$ is the largest eigenvalue of the flux Jacobian, df/du, evaluated on the local domain of (u_j,u_{j+1}). The first-order local Lax-Friedrichs flux is defined as

$$\hat{f}_{j+1/2}=f^{+}_{j+1/2}(u_j)+f^{-}_{j+1/2}(u_{j+1}) \tag{7}$$

Then, the high order ENO flux is obtained as

$$f^{+}_{j+1/2}(u)=\frac{1}{2}\left(f\left(u[x_j]\right)+\alpha_{j+1/2}u[x_j]\right),$$

$$f^{-}_{j+1/2}(u)=\frac{1}{2}\left(f\left(u[x_j]\right)-\alpha_{j+1/2}[x_j]\right) \tag{8}$$

It is straight forward to obtain a polynomial reconstruction to a order of accuracy greater than two. The formulation based on the Convex ENO scheme [10] uses the divided difference values closest to the previous order of fluxes chosen. The scheme reduces to a low-order automatically at discontinuities, while it maintains a higher-order in the smooth region.

Physical description of interface tracking

A level-set method [1,11] provides a simple way to track a multi-material interface that may separate a gas from a solid, for example. We consider the material interface of 1) gas-gas, 2) gas-liquid, 3) solid-solid, and 4) solid-void (vacuum). The sharp discontinuity of state variables across the interface is handled using the level sets. The level-set equation in two dimension below tracks the location of the material interface represented by the zero-level contour $\phi(x,y)=0$,

$$\frac{\partial\phi}{\partial t}+v_1\frac{\partial\phi}{\partial x}+v_2\frac{\partial\phi}{\partial y}=0 \tag{9}$$

Initially, ϕ is taken as the signed normal distance function to the interface. The material interface evolves with local material velocity, $v=(v_1,v_2)$. The material velocity on either side of the interface provides the velocity extension that is used for advection of ϕ in the level-set domain. The level-set function, ϕ, is taken positive outside of material and negative inside, and ϕ is initialized to be a signed normal distance from the material interface.

The re-initialization of level-set contours is a necessary procedure for making sure that no steep gradient enters into the smooth level-set field of a distance function, ϕ. This requires solving the following equations until a steady state is reached:

$$\phi_\tau + S(\phi)\left(|\nabla\phi| - 1\right) = 0 \tag{10}$$

where the smeared sign function, $S = \frac{\phi}{\sqrt{\phi^2 + \left(1 - |\nabla\phi|\right)^2 \Delta x^2}}$ is used from [11]. Then equation (10) is solved by the Godunov's scheme as:

$$\begin{aligned}\phi^{n+1} &= \phi^n \\ &- \tfrac{\Delta\tau}{\Delta x} S^+ \left(\sqrt{\max[(a^+)^2, (b^-)^2] + \min[(c^+)^2, (d^-)^2]} - 1\right) \\ &- \tfrac{\Delta\tau}{\Delta x} S^- \left(\sqrt{\max[(a^-)^2, (b^+)^2] + \min[(c^-)^2, (d^+)^2]} - 1\right)\end{aligned} \tag{11}$$

where $a^\pm, b^\pm, c^\pm, d^\pm$ are the Gudunov fluxes from [11]. The monotonicity of equation (11) is enforced by restricting the time step as follows

$$\frac{\Delta\tau}{\Delta x}|S| \le \frac{1}{2} \tag{12}$$

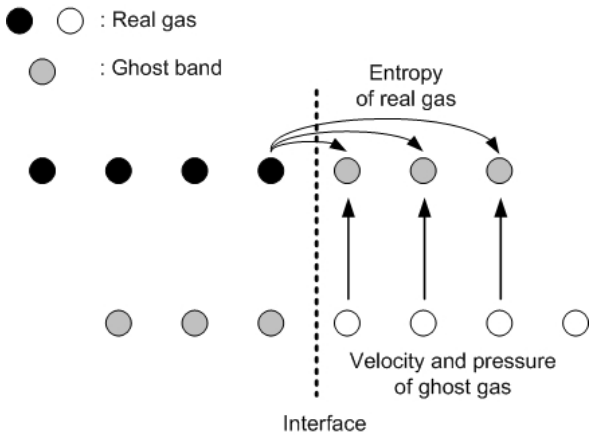

Fig. 1 Original 1-D ghost fluid conditions for contact of two materials with no strength (e.g. two gases)

Gas-gas interface tracking

In many of the gas dynamics simulations, a single phase gas is assumed for simulating the phenomena of interest. In a physical system simulation, it is natural to include the multi-gas effects. At the gas-gas interface, the entropy and density jump while velocity and pressure are continuous. This jump in entropy and density provides an extra strain on the calculation of interface evolution. The ghost fluid concept is used to remedy the inherent oscillatory behavior of the interface. We let two gases evolve independent of each other so as to solve a set of two Riemannn problems (see figure 1). A band of ghost points on the other side of real gas defines a natural boundary condition for the real gas. The equation of state is then used to calculate the internal energy of the ghost point.

Using the physical condition that pressure and velocity are continuous across the material interface, we set the velocity and pressure of the ghost band of the real gas equal to the velocity and pressure of the ghost gas. Once the pressure and velocity have been defined in the ghost band, we need to specify one more quantity to define a material. We use one sided extrapolation of entropy which would minimize the dissipative error associated with the sharp density gradient. To further suppress any spurious oscillation from the well-known over-heating effect [12], the isobaric fix is applied in a way that defines velocity, pressure and entropy (or density) of the ghost band in one-dimension as

$$v_{i+1}\big|_{\text{mat1}}^{\text{ghost}} = v_{i+1}\big|_{\text{mat2}}^{\text{real}},\ p_{i+1}\big|_{\text{mat1}}^{\text{ghost}} = p_{i+1}\big|_{\text{mat2}}^{\text{real}} \tag{13}$$

$$\rho_{i+1}\big|_{\text{mat1}}^{\text{ghost}} = \rho_i\big|_{\text{mat1}}^{\text{real}} \left(p_{i+1}\big|_{\text{mat1}}^{\text{ghost}} / p_i\big|_{\text{mat1}}^{\text{real}}\right)^{1/\gamma_{real}} \tag{14}$$

where we have used the definition of entropy $\eta = p/\rho^\gamma$ for ideal gas. The two-dimensional extension of the ghost node procedure for smooth variables (v_n, p), discontinuous variable (v_t), and extrapolated variables (ρ or e) will be discussed in the general solid-solid case.

Gas-water interface tracking

The interaction of gas-water interface can be found in a whole class of problems that include the underwater explosion with cavitations. In this case, the velocity and pressure are obtained using (13) as in the gas-gas case while the density is not the extrapolation variable in this case. Since the equation of state for water has pressure as a function only of density ($p = B\left(\frac{\rho}{\rho_0}\right)^\gamma - B + A$, $\gamma = 7.15$, $A = 10^5\,\text{Pa}$, $B = 3.31\times10^8\,\text{Pa}$, and $\rho_0 = 1{,}000\,\text{kg/m}^3$), one needs to be careful when choosing the isobaric fix variable. A natural choice for water is the internal energy whereas the entropy was used for gas previously. In the ghost band region, the ghost variables are then defined as follows:

$$v_{i+1}\big|_{\text{mat1}}^{\text{ghost}} = v_{i+1}\big|_{\text{mat2}}^{\text{real}},\ p_{i+1}\big|_{\text{mat1}}^{\text{ghost}} = p_{i+1}\big|_{\text{mat2}}^{\text{real}} \tag{15}$$

$$e_{i+1}\big|_{\text{mat1}}^{\text{ghost}} = e_{i+1}\big|_{\text{mat2}}^{\text{real}} \tag{16}$$

The two-dimensional extension of the smooth variables, discontinuous variables, and extrapolated variables are discussed in the following solid-solid section.

Solid-solid interface tracking

In [3], authors proposed a simple algorithm to calculate the interaction between two metals. They pointed out that the original ghost fluid concept of [1] cannot be applied to describe the motion of strong impacts of metals because the deviatoric stresses introduced in the elasto-plastic material affect the effective pressure and the density. Since the original ghost fluid concept would work properly in the low strain-rate deformation, the original concept is extended to incorporate the physical restrictions such as the Rankine-Hugoniot relations and the approximate Riemann solver. In this work, we introduce an extended ghost fluid concept for describing the elasto-plastic behavior of metals in contact.

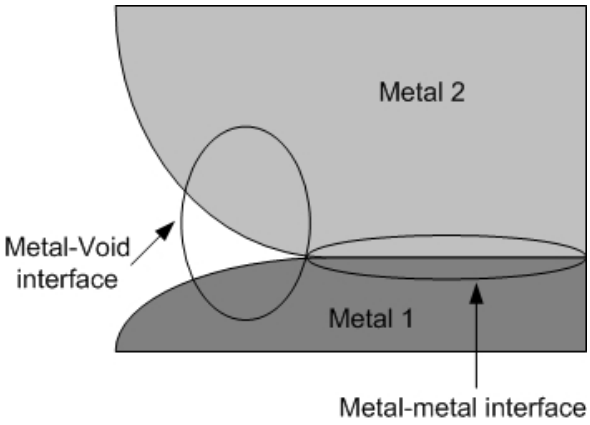

Fig. 2 Two-dimensional contact of materials with strength (e.g. two metal)

Along the metal-metal interface shown in figure 2, we impose continuous local velocity normal to the interface and the continuous normal traction. However, the shear and tangential components of traction remain discontinuous. Thus the variables of ghost band are obtained via the combination of the ghost fluid concept and the physical restrictions. First, the ghost point (G) at (i, j) of metal-metal interface in figure 3 is found, and the normal unit vector of the level-set function is computed. Then, the reflected point (R) adjacent to the ghost point from the combination of the ghost and unit normal vector is obtained. Then one determines whether the fixed nodes around the reflected point (R) is real or ghost. From this procedure, one can identify the reflected point and evaluate its value by the bilinear interpolation. The interpolation is performed using the following simple relation for three fixed nodes,

$$U_R = U_{i+1,j}(1-Y) + U_{i+1,j+1}(X+Y-1) + U_{i,j+1}(1-X) \tag{17}$$

where $X = (x - x_i)/\Delta x$ and $Y = (y - y_j)/\Delta y$.

We apply the physical restriction to the obtained ghost point values. The normal and tangential velocities are defined as

$$v_n\big|_{\text{mat1}}^{\text{ghost}} = \left(v_x n_x + v_y n_y\right)\Big|_{\text{mat2}}^{\text{real}} \tag{18}$$

$$v_t\big|_{\text{mat1}}^{\text{ghost}} = \left(v_x n_y - v_y n_x\right)\Big|_{\text{mat1}}^{\text{real}} \tag{19}$$

Because the velocity normal to the interface is continuous and the tangential velocity is discontinuous, the components of the normal and the tangential velocities are directly related to the real and the ghost velocity components, respectively (see equations (18,19)). The obtained velocity components are converted to the Cartesian components via the following relations

$$v_x\big|_{\text{mat1}}^{\text{ghost}} = \left(v_n n_x + v_t n_y\right)\Big|_{\text{mat1}}^{\text{ghost}} \tag{20}$$

$$v_y\big|_{\text{mat1}}^{\text{ghost}} = \left(v_n n_y - v_t n_x\right)\Big|_{\text{mat1}}^{\text{ghost}} \tag{21}$$

Density and internal energy of the ghost point are extrapolated from the reflected point. Finally the pressure is obtained by the equation of the state which relates density and internal energy.

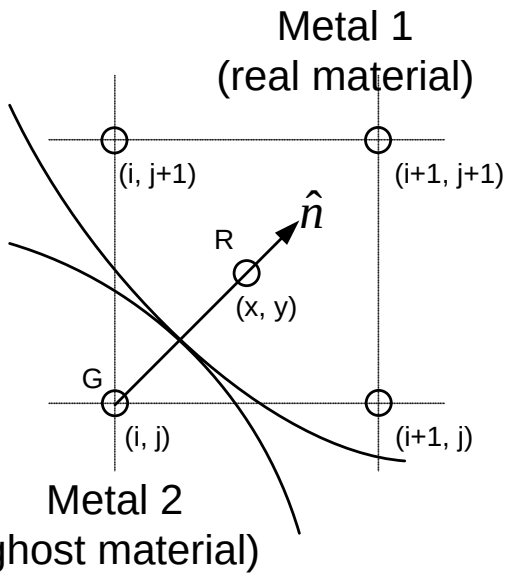

Fig. 3 Schematic of 2-D ghost fluid conditions for solid-solid case

Additional variables of deviatoric stress and effective plastic strain at the ghost point are also obtained from the physical restrictions of the ghost fluid concept. To find the deviatoric stress components, the Cauchy stress components at the ghost point are first determined:

$$\sigma_{nn}\big|_{\text{mat1}}^{\text{ghost}} = \left(n_x^2 s_{xx} + n_y^2 s_{yy} + 2n_x n_y s_{xy} - p\right)\Big|_{\text{mat2}}^{\text{real}} \tag{22}$$

$$\sigma_{tt}\big|_{\text{mat1}}^{\text{ghost}} = \left(n_x^2 s_{yy} + n_y^2 s_{xx} - 2n_x n_y s_{xy} - p\right)\Big|_{\text{mat1}}^{\text{real}} \tag{23}$$

$$\sigma_{nt}\big|_{\text{mat1}}^{\text{ghost}} = \left(n_x n_y (s_{yy} - s_{xx}) + (n_x^2 - n_y^2) s_{xy}\right)\Big|_{\text{mat2}}^{\text{real}} \tag{24}$$

The continuity of the normal traction is enforced while the shear and tangential tractions are left discontinuous. The components of deviatoric stresses are found as

$$s_{xx}\big|_{\text{mat1}}^{\text{ghost}} = \left(n_x^2 \sigma_{nn} + n_y^2 \sigma_{tt} - 2n_x n_y \sigma_{nt} - p\right)\Big|_{\text{mat1}}^{\text{ghost}} \tag{25}$$

$$s_{yy}\big|_{\text{mat1}}^{\text{ghost}} = \left(n_x^2 \sigma_{nn} + n_y^2 \sigma_{tt} + 2n_x n_y \sigma_{nt} - p\right)\Big|_{\text{mat1}}^{\text{ghost}} \tag{26}$$

$$s_{xy}\big|_{\text{mat1}}^{\text{ghost}} = \left(n_x n_y (\sigma_{nn} - \sigma_{tt}) + (n_x^2 - n_y^2)\sigma_{nt}\right)\Big|_{\text{mat1}}^{\text{ghost}} \tag{27}$$

We extrapolate the effective plastic strain from the reflected point such that

$$\bar{\varepsilon}^p\big|_{\text{mat1}}^{\text{ghost}} = \bar{\varepsilon}^p\big|_{\text{mat1}}^{\text{real}} \tag{28}$$

implying that the ghost point at (i, j) is defined by its reflected twin (R) in figure 3.

Solid-void interface tracking

For the metal-void interface shown in figure 4, we apply the zero traction normal and shear to the interface, but allow the tangential traction to slip. As in the case of metal-metal, the metal-void procedure for obtaining the ghost variables is identical. We first compute the unit normal vector from the level-set function and find the reflected point using the unit

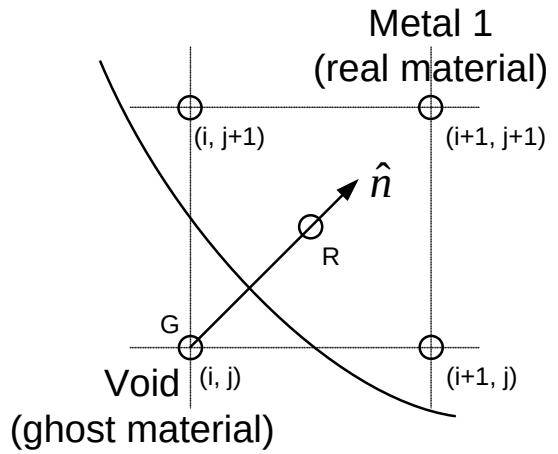

Fig. 4 Schematic of 2-D ghost fluid conditions for solid-Void case

normal vector and the ghost point as discussed in the previous section. The Cartesian components of ghost velocities are given in equations (20, 21).

Next, we require that the normal and shear components of the traction are zero and the tangential traction is discontinuous such that

$$\sigma_{nn}\big|_{\text{mat1}}^{\text{ghost}} = 0\,,\ \sigma_{nt}\big|_{\text{mat1}}^{\text{ghost}} = 0 \tag{29}$$

$$\sigma_{tt}\big|_{\text{mat1}}^{\text{ghost}} = \left(n_x^2 s_{yy} + n_y^2 s_{xx} - 2n_x n_y s_{xy} - p\right)\Big|_{\text{mat1}}^{\text{real}} \tag{30}$$

The resulting deviatoric stress terms at the ghost point in the Cartesian coordinate are

$$s_{xx}\big|_{\text{mat1}}^{\text{ghost}} = \left(n_y^2\sigma_{tt} - p\right)\Big|_{\text{mat1}}^{\text{ghost}} \tag{31}$$

$$s_{yy}\big|_{\text{mat1}}^{\text{ghost}} = \left(n_x^2\sigma_{tt} - p\right)\Big|_{\text{mat1}}^{\text{ghost}} \tag{32}$$

$$s_{xy}\big|_{\text{mat1}}^{\text{ghost}} = \left(-n_x n_y\sigma_{tt}\right)\Big|_{\text{mat1}}^{\text{ghost}} \tag{33}$$

As before, the effective plastic strain at the ghost point (i, j) is given by equation (28).

Equations

Multi-step chemical reaction

For illustration of the numerical implementation of multi-step chemistry, we consider the following two first order reactions and one second-order reaction:

$$A \xrightarrow{r_1} B$$
$$B \xrightarrow{r_2} C \tag{34}$$
$$C \xrightarrow{r_3} D$$

where the three reaction rates are for each steps of reaction,

$$r_1 = Z_1 \exp(-E_1/RT)\rho_A$$
$$r_2 = Z_2 \exp(-E_2/RT)\rho_B$$
$$r_3 = Z_3 \exp(-E_3/RT)\rho_C^2 \tag{35}$$

Here A is the unreacted solid energetic material, B is a solid-state intermediate, C and D are intermediate and final product gases, respectively. Each i -th chemical reaction follows the Arrhenius form with the reaction rate- r_i , the frequency factor- Z_i , the activation energy- E_i , and the j -th species density, ρ_j . The mass conservation requires that $\rho = \rho_A + \rho_B + \rho_C + \rho_D$. The species equations then become

$$\frac{D\rho_A}{Dt} = -r_1, \frac{D\rho_B}{Dt} = r_1 - r_2, \frac{D\rho_C}{Dt} = r_2 - r_3, \frac{D\rho_D}{Dt} = r_3 \tag{36}$$

with D/Dt , the total derivative.

The solutions to the four-species reaction equations in (36) is obtained by the linearized implicit ODE integrator that does not require matrix inversion of the source Jacobian matrix associated with the standard iterative procedure. The incremental change in the species production per time step is calculated by the linearized implicit Runge-Kutta scheme [8]

$$U^{n+1} = U^n + \sum_{j=1}^{r} W_j k_j$$

$$[I - \Delta t d_i \frac{\partial W}{\partial U}(U^n + \sum_{j=1}^{i-1} c_{ij}k_j)]k_i = \Delta t W(U^n + \sum_{j=1}^{i-1} c_{ij}k_j)$$

$$(i = 1,\ldots,3) \tag{37}$$

where the species vector is $U = (\rho_A, \rho_B, \rho_C, \rho_D)$ and the species source vector is $W = (-r_1, r_1 - r_2, r_2 - r_3, r_3)$. The source Jacobian needed in the integration of the species reaction process is evaluated for the three-step reactions:

$$\frac{\partial W}{\partial U} = \begin{bmatrix} \frac{\partial W_A}{\partial U_A} = \frac{-r_1}{\rho_A} & \frac{\partial W_A}{\partial U_B} = 0 & \frac{\partial W_A}{\partial U_C} = 0 & \frac{\partial W_A}{\partial U_D} = 0 \\ \frac{\partial W_B}{\partial U_A} = \frac{r_1}{\rho_A} & \frac{\partial W_B}{\partial U_B} = \frac{-r_2}{\rho_B} & \frac{\partial W_B}{\partial U_C} = 0 & \frac{\partial W_B}{\partial U_D} = 0 \\ \frac{\partial W_C}{\partial U_A} = 0 & \frac{\partial W_C}{\partial U_B} = \frac{r_2}{\rho_B} & \frac{\partial W_C}{\partial U_C} = \frac{-2r_3}{\rho_C} & \frac{\partial W_C}{\partial U_D} = 0 \\ \frac{\partial W_D}{\partial U_A} = 0 & \frac{\partial W_D}{\partial U_B} = 0 & \frac{\partial W_D}{\partial U_C} = \frac{2r_3}{\rho_C} & \frac{\partial W_D}{\partial U_D} = 0 \end{bmatrix} \tag{38}$$

Burn(deflagration) propagation

During the burning of condensed phase energetic material, the surface regression is assumed to vary with respect to pressure such that

$$v_n = ap^n \tag{39}$$

where the surface normal velocity v_n propagates the burning surface into the unreacted solid explosive as the n-th power of pressure. The regression coefficient-a, power coefficient-n are summarized for HMX and RDX [13,14]. When 20% of final product gas is produced, the finite chemical kinetics is no longer solved; instead a switch in chemical step is

made to simply propagate the burning front via Jacobi-Hamilton equation of the form

$$\phi_t + v_n \phi_n = 0 \tag{40}$$

where ϕ is a passive scalar called the level sets that defines and propagates the burning boundary between the reacted and unreacted condensed energetics.

2. JWL++ model for detonation

High explosives generate a high pressure (~10 GPa) shock wave (~5 km/s) with a typical detonation time scale ranging in several micro-seconds. Improved from the classical fast detonative kinetic model of Ignition and Growth [15], a simpler JWL++ model [16] consists of four parts: unreacted HE pressure, reacted HE pressure, a mixer of two pressures, and simple reaction rate equation. Pressure of the unreacted HE is expressed by the Murnaghan equation as:

$$p_{unreacted} = \frac{1}{n\kappa}\left(\frac{1}{v^n} - 1\right) \tag{41}$$

where $v = \rho / \rho_0$ and n, κ are material dependent parameters. For example, n = 7.4, $\kappa = 39 \times 10^{-11} Pa^{-1}$, and $\rho_0 = 1160 kg/m^3$ are used for ANFO-K1.

The pressure of reacted HE is given by:

$$p_{reacted} = A\exp(-R_1 v) + B\exp(-R_2 v) + \frac{C}{\rho_0 \kappa v^{n-1}} \tag{42}$$

where A, B, C, R_1, R_2, ρ_0 and κ are material dependent parameters given in Table 1 of Ref. [17].

For the mixer of two equations of state, a simpler algorithm based on the mixture theory is used. It is known that the mixer is not the critical factor to a detonation initiation. The pressure is obtained by:

$$p_{mix} = (1-\lambda) p_{unreacted} + \lambda p_{reacted} \tag{43}$$

where the mass fraction of product, λ, is a reaction progress variable that is governed by the global rate equation of the form

$$\frac{d\lambda}{dt} = G(p+q)^b (1-\lambda) \tag{44}$$

with the reaction rate constant $G = 3.5083 \times 10^{-7} s^{-1} Pa^{-b}$, pressure power constant $b = 1.3$ and artificial viscous constant $q = 0$ for ANFO-K1, for example.

Model equations for gaseous phase energetic simulation

The two-dimensional, conservative hyperbolic equation for reactive compressible flow in equation (1) consists of the conservative vectors given by

$$U = \begin{bmatrix} \rho \\ \rho v_1 \\ \rho v_2 \\ \rho E \\ \rho_i \end{bmatrix}, \; F = \begin{bmatrix} \rho v_1 \\ \rho v_1^2 + p \\ \rho v_1 v_2 \\ v_1(\rho E + p) \\ \rho_i v_1 \end{bmatrix}, \; G = \begin{bmatrix} \rho v_2 \\ \rho v_1 v_2 \\ \rho v_2^2 + p \\ v_2(\rho E + p) \\ \rho_i v_2 \end{bmatrix} \tag{45}$$

with a source term vector

$$W = \begin{bmatrix} 0 \\ 0 \\ 0 \\ -\nabla \vec{q} - \sum_{i=1}^{N} r_i q_i \\ w_i \end{bmatrix} \tag{46}$$

where ρ_i is the partial density of each i-th HE compositions (summing up to a total density, ρ), $\vec{q}$ is the heat flux, and q_i is the heat of reaction.

Model equations for condensed phase energetics and metallic (inert) confinements

The inclusion of deviatoric stresses and effective plastic strain to the above formulation is considered. The governing variables are given by

$$u = \begin{bmatrix} \rho \\ m \\ n \\ r \\ \alpha \\ \beta_i \end{bmatrix} = \begin{bmatrix} \rho \\ \rho v_1 \\ \rho v_2 \\ \rho E \\ \rho \lambda \\ \rho \phi_i \end{bmatrix} \tag{47}$$

where i = 1, …, 4, and ϕ_i represents the three deviatoric stress components s_{ij} and the effective plastic strain $\bar{\varepsilon}^p$. As before, λ is a single product mass fraction that monitors the extent of reaction. The conservative fluxes in x, y directions then become

$$f = \begin{bmatrix} m \\ m^2/\rho + p \\ mn/\rho \\ m(r+p)/\rho \\ \alpha m/\rho \\ \beta_i m/\rho \end{bmatrix}, \; g = \begin{bmatrix} n \\ mn/\rho \\ n^2/\rho + p \\ n(r+p)/\rho \\ \alpha n/\rho \\ \beta_i n/\rho \end{bmatrix} \tag{48}$$

In the dynamic response of metals without chemical reaction, α would remain zero. The equation of state for obtaining the pressure or the traceless component of stress tensor is obtained via a choice of model equations for both energetic and inert materials. The source that models the elasto-plastic behavior of a typical metal is

$$W=\begin{bmatrix} 0 \\ \dfrac{\partial s_{xx}}{\partial x}+\dfrac{\partial s_{xy}}{\partial y} \\ \dfrac{\partial s_{xy}}{\partial x}+\dfrac{\partial s_{yy}}{\partial y} \\ \dfrac{\partial}{\partial x}(v_1 s_{xx}+v_2 s_{xy}-q_x)+\dfrac{\partial}{\partial y}(v_1 s_{xy}+v_2 s_{yy}-q_y) \\ \rho\left(2\mu\left(D_{xx}{}'-\dfrac{3}{2}\dfrac{s_{xx}}{\bar{\sigma}}\dot{\bar{\varepsilon}}^{p}\right)\right)+\Omega_{xm}s_{mx}-s_{xm}\Omega_{mx} \\ \rho\left(2\mu\left(D_{yy}{}'-\dfrac{3}{2}\dfrac{s_{yy}}{\bar{\sigma}}\dot{\bar{\varepsilon}}^{p}\right)\right)+\Omega_{ym}s_{my}-s_{ym}\Omega_{my} \\ \rho\left(2\mu\left(D_{xy}{}'-\dfrac{3}{2}\dfrac{s_{xy}}{\bar{\sigma}}\dot{\bar{\varepsilon}}^{p}\right)\right)+\Omega_{xm}s_{my}-s_{xm}\Omega_{my} \\ \rho\left(\dfrac{1}{1+H'/(3\mu)}\dfrac{s_{xx}D_{xx}{}'+s_{yy}D_{yy}{}'+2s_{xy}D_{xy}{}'}{\bar{\sigma}}\right) \end{bmatrix} \quad (49)$$

where the last four terms of source vector W corresponds to the three components of deviatoric stress s_{xx}, s_{xy}, s_{yy} and the effective plastic strain $\bar{\varepsilon}^{p}$. The detailed derivation of these equations is given in [17].

Time step control

The control of the time step increment during the multi-material reactive simulation follows two basic modes of operation: 1) fixed time step that uses the specified time increment for each cycle, and 2) time constraints that the code automatically chooses as appropriate time step based on numerical properties of the dynamic simulation.

In the fixed time step control mode, the user defined time increment represents a physically allowable minimum value that would reasonably resolve dynamic events taking place during the reactive multi-material flow. This would require experience and a good sense of problem intuition toward the expected solution behavior. Oftentimes, smallest allowable time step increment is used to avoid noises present in the flow field of multi-scale (time and space) simulation.

In the constraint approach that is discussed in detail below, the step size control decision is based on the constraints of hydrodynamics, thermal transport, and chemistry. For explicit time marching, a stability condition for thermal diffusion is given by

$$\Delta t_{therm}=\frac{1}{2}\frac{\rho c_v(\Delta x)^2}{k} \quad (50)$$

with c_v, k being heat capacity and thermal conductivity, respectively.

Two controls are used to define the amount of reaction that is allowed during a time step. During the part of a chemical reaction run where reactions are occurring slowly, high fidelity on the chemical composition is desired. A small change in the composition can have significant noise on the final results. When the reactions are occurring rapidly, all that is modeled is a rapid transformation from reactant to product. The non-linear aspect of chemical reactions is their temperature dependence.

During the species reaction process, numerical difficulties arise when the chemical reaction timescale to other phenomena occurring in a system is much smaller than 1. In other words, the large cell Damkohler number ($Da=\Delta t_{CFL}/\Delta t_{chem}$) of chemical reaction processes is associated with the sufficiently small chemical relaxation time scale τ that is inversely proportional to the large pre-exponential factor Z_i. The sub-cycle time step Δt_{chem} required to accurately resolve chemical relaxation within a single cycle of Δt_{CFL} step is chosen in the range of $O(\tau)\sim O(\Delta x)$ for numerically efficient and stable calculation for either explicit or implicit time integration.

Advection puts limit on amount of material that can flow through a grid in one time step. This is the case where the appropriate time scale for advection Δt scales as $\sim O(\Delta x)$, the grid size. The CFL condition monitors the domain of influence of the characteristic wave speeds based on the convective Jacobian matrices of the hyperbolic system in (1). In two dimensions, the CFL time step is calculated from

$$\Delta t_{CFL}=CFL\times\min\left\{\frac{\Delta x}{\max|df/du|},\frac{\Delta y}{\max|dg/du|}\right\} \quad (51)$$

where CFL is the Courant number, $\max|df/du|$ and $\max|dg/du|$ are the largest eigenvalues (in absolute sense) of the Jacobians of f and g. Evaluation of the derivatives of f and g with respect to u give

$$\frac{df}{du}=\begin{bmatrix} 0 & 1 & 0 & 0 & 0 & 0 \\ -\dfrac{m^2}{\rho^2}+\dfrac{\partial p}{\partial \rho} & \dfrac{2m}{\rho}+\dfrac{\partial p}{\partial m} & \dfrac{\partial p}{\partial n} & \dfrac{\partial p}{\partial r} & \dfrac{\partial p}{\partial \alpha} & \dfrac{\partial p}{\partial \beta_i} \\ -\dfrac{mn}{\rho^2} & \dfrac{n}{\rho} & \dfrac{m}{\rho} & 0 & 0 & 0 \\ -\dfrac{m}{\rho^2}(r+p)+\dfrac{m}{\rho}\dfrac{\partial p}{\partial \rho} & \dfrac{r+p}{\rho}+\dfrac{m}{\rho}\dfrac{\partial p}{\partial m} & \dfrac{m}{\rho}\dfrac{\partial p}{\partial n} & \dfrac{m}{\rho}\left(1+\dfrac{\partial p}{\partial r}\right) & \dfrac{m}{\rho}\dfrac{\partial p}{\partial \alpha} & \dfrac{m}{\rho}\dfrac{\partial p}{\partial \beta_i} \\ -\dfrac{\alpha m}{\rho^2} & \dfrac{\alpha}{\rho} & 0 & 0 & \dfrac{m}{\rho} & 0 \\ -\dfrac{\beta_i m}{\rho^2} & \dfrac{\beta_i}{\rho} & 0 & 0 & 0 & \dfrac{m}{\rho} \end{bmatrix} \quad (52)$$

and

$$\frac{dg}{du}=\begin{bmatrix} 0 & 0 & 1 & 0 & 0 & 0 \\ -\dfrac{mn}{\rho^2} & \dfrac{n}{\rho} & \dfrac{m}{\rho} & 0 & 0 & 0 \\ -\dfrac{n^2}{\rho^2}+\dfrac{\partial p}{\partial \rho} & \dfrac{\partial p}{\partial m} & \dfrac{2n}{\rho}+\dfrac{\partial p}{\partial n} & \dfrac{\partial p}{\partial r} & \dfrac{\partial p}{\partial \alpha} & \dfrac{\partial p}{\partial \beta_i} \\ -\dfrac{n}{\rho^2}(r+p)+\dfrac{n}{\rho}\dfrac{\partial p}{\partial \rho} & \dfrac{n}{\rho}\dfrac{\partial p}{\partial m} & \dfrac{r+p}{\rho}+\dfrac{n}{\rho}\dfrac{\partial p}{\partial n} & \dfrac{n}{\rho}\left(1+\dfrac{\partial p}{\partial r}\right) & \dfrac{n}{\rho}\dfrac{\partial p}{\partial \alpha} & \dfrac{n}{\rho}\dfrac{\partial p}{\partial \beta_i} \\ -\dfrac{\alpha n}{\rho^2} & 0 & \dfrac{\alpha}{\rho} & 0 & \dfrac{n}{\rho} & 0 \\ -\dfrac{\beta_i n}{\rho^2} & 0 & \dfrac{\beta_i}{\rho} & 0 & 0 & \dfrac{n}{\rho} \end{bmatrix} \quad (53)$$

The eigenvalues of the Jacobians (40) and (41) are

$$\lambda^f = v_1 - c, v_1, v_1, v_1, v_1, v_1 + c,$$
$$\lambda^g = v_2 - c, v_2, v_2, v_2, v_2, v_2 + c \quad (54)$$

where the sound speed c is defined by

$$c^2 = \frac{\partial p}{\partial \rho} + \frac{p}{\rho^2}\frac{\partial p}{\partial e} \quad (55)$$

The partial derivatives of pressure in the case of an ideal EOS given as $p = (\gamma - 1)\{r - (m^2 + n^2)/(2\rho)\}$ are determined:

$$\frac{\partial p}{\partial \rho} = (\gamma - 1)\frac{m^2 + n^2}{2\rho^2},\ \frac{\partial p}{\partial m} = -(\gamma - 1)\frac{m}{\rho},$$
$$\frac{\partial p}{\partial n} = -(\gamma - 1)\frac{n}{\rho},\ \frac{\partial p}{\partial r} = \gamma - 1,\ \frac{\partial p}{\partial \alpha} = 0,\ \frac{\partial p}{\partial \beta_i} = 0 \quad (56)$$

For an ideal EOS for HE, $p = (\gamma - 1)\{r + Q_c\alpha - (m^2 + n^2)/(2\rho)\}$ with a heat of combustion Q_c, the partial derivatives are found as

$$\frac{\partial p}{\partial \rho} = (\gamma - 1)\frac{m^2 + n^2}{2\rho^2},\ \frac{\partial p}{\partial m} = -(\gamma - 1)\frac{m}{\rho},$$
$$\frac{\partial p}{\partial n} = -(\gamma - 1)\frac{n}{\rho},\ \frac{\partial p}{\partial r} = \gamma - 1,\ \frac{\partial p}{\partial \alpha} = (\gamma - 1)Q_c,$$
$$\frac{\partial p}{\partial \beta_i} = 0 \quad (57)$$

In the case of Mie-Gruneisen EOS for metal, the pressure is given by

$$p = \Gamma\left[r - \frac{1}{2\rho}\left(m^2 + n^2\right)\right] + \frac{\rho_0 c_0^2 \varphi}{(1 - s\varphi)^2}\left[1 - \frac{\Gamma}{2v}(v_0 - v)\right] \quad (58)$$

with $\varphi = 1 - v/v_0$ where v is the specific volume. The partial derivatives of pressure become

$$\frac{\partial p}{\partial \rho} = \Gamma\frac{m^2 + n^2}{2\rho^2} + \rho_0 c_0^2\left[\frac{v^2}{v_0}\frac{C_2}{(C_1)^2} + 2s\left(\frac{v}{v_0}\right)^2\frac{(v_0 - v)C_2}{(C_1)^3} - \frac{\Gamma(v_0 - v)}{2(C_1)^2}\right],$$
$$\frac{\partial p}{\partial m} = -\frac{\Gamma}{\rho}m,\ \frac{\partial p}{\partial n} = -\frac{\Gamma}{\rho}n,\ \frac{\partial p}{\partial r} = \Gamma,\ \frac{\partial p}{\partial \alpha} = 0,$$
$$\frac{\partial p}{\partial \beta_i} = 0 \quad (59)$$

With $C_1 = 1 - s\varphi$, $C_2 = 1 - \frac{\Gamma}{2v}(v_0 - v)$. Thus the optimal time step Δt_{CFL} is obtained by picking the larger of the eigenvalues in λ^f and λ^g. This procedure will assure that the domain of influence is properly covered by the computational mesh in space-time.

Verification of convergence

We consider two different gases initially brought to a contact. Upon removal of the diaphragm between the gases with different γ's, an expansion wave and a shock propagate in the opposite direction, and a material interface follows the right-running shock. Listed in Table 1 are the initial conditions of this exercise. 100 points spanning 1 meter in x-direction is used in this shock tube calculation. The spatial accuracy of a fourth-order convex ENO scheme with a third-order Runge-Kutta scheme is tested for its rate of convergence. The material interface between the gases is tracked via the ghost fluid approach adapted in the Hydro-SCCM.

The spatial accuracy is analyzed by measuring the relative error E_1 in the L_1 norm during the time integration for estimating the rate of convergence. The eight data points between x =0.52 to x =0.59 in increments of Δx =0.01 are compared with the double grid data points at the same locations at time t=0.0007. The discrete L_1 norm is defined as:

$$E_1 = \sum_i \left|\rho^{exact} - \rho_i\right| \Delta x \quad (60)$$

If a method is of r-th order, then for a uniform mesh with N grid points, the error satisfies

$$E_1^N = \mathrm{O}\left(\Delta x^{r_c}\right) \quad (61)$$

When the uniform mesh is refined by doubling the grid points, we should have

$$E_1^{2N} = \mathrm{O}\left(\left(\frac{\Delta x}{2}\right)^{r_c}\right) \quad (62)$$

Then, one can solve for the rate of convergence, r_c and finds

$$r_c = \frac{\ln E_1^N - \ln E_1^{2N}}{\ln 2} \quad (63)$$

The L_1 error and the rate of convergence based on density are displayed in Table 2 with the rate of convergence calculated.

In this convergence test using the fourth-order convex ENO scheme with the material interface tracking algorithm used in the Hydro-SCCM, we have shown that the rate of convergence approaches the theoretical value of 4, each time grids are refined. In order to minimize the possible error due to the use of a third-order temporal algorithm, Δt is kept small compared to Δx.

Table. 1 Initial conditions for convergence test

	Gas1 (50 cm)	Gas2 (50 cm)
γ	1.4	1.2
ρ(kg/m^3)	1	0.125
p(Pa)	1.5 x 10^5	1.0 x 10^4
v(m/s)	0	0

Table. 2 Initial conditions for convergence test

N	E_1	r_c
100	9.0×10^{-5}	-
200	1.68×10^{-5}	2.4
400	2.7×10^{-6}	2.8
800	1.8×10^{-7}	3.9

Conclusion

We have presented a numerical methodology utilized in the development of the Hydro-SCCM tool for computing multi-material shock physics at slow to high speed dynamics involving high explosives and inert confinements. Chemical reaction models include both deflagration and detonation of condensed phase energetic materials. The developed tool is useful for analysis of an energetic system interacting with chemico-mechanical shock loadings in both gaseous and condensed phase media that is confined by the elasto-plastically deforming boundaries. The extended and applied utilization of the tool is the subject of the companion paper.

Acknowledgments

The authors are grateful to a list of funding agencies through which the projects HEMRC-HM-20 and KRF-2006-311-D0038 were conducted. The additional support from the Brain Korea 21 through the Institute of Advance Aerospace Technology at the Seoul National University is also acknowledged.

References

1) Fedkiw, R.P., Aslam, T., Merriman, B., and Osher, S.: A Non-oscillatory Eulerian Approach to Interface in Multimaterial Flows(The Ghost Fluid Method), *Journal of Computational Physics*, **152**, 1999, pp. 457-492.
2) Stewart, D.S., Yoo, S., and Wescott, B.L.: High-order Numerical Simulation and Modeling of the Interaction of Energetic and Inert Materials, *Combustion Theory and Modelling*, **11**, 2007, pp. 305-332.
3) Tran, L. and Udaykumar, H.S.: A particle-level set-based Sharp Interface Cartesian Grid Method for Impact, Penetration, and Void Collapse, *Journal of Computational Physics*, **193**, 2004, pp. 469-510.
4) Liu, T.G., Khoo, B.C., and Yeo, K.S.: Ghost Fluid Method for Strong Shock Impacting on Material Interface, *Journal of Computational Physics*, **190**, 2003, pp. 651-681.
5) McGlaun, J.M., Thompson, S.L., and Elrick, M.G.: CTH: a Three-dimensional Shock Wave Physics code, *International Journal of Impact Engineering*, **10**, 1990, pp. 351-360.
6) Sharp, R. and the ALE3D Team, Users Manual for ALE3D, Lawrence Livermore National Laboratory, 2003, Ver. 3.6.1.
7) Kothe, D.B., Baumgardner, J.R., et al., PAGOSA: A Massively-Parallel, Multi-Material Hydrodynamics Model for Three-Dimensional High-Speed Flow and High-Rate Material Deformation, High Performance Computing Symposium, 1993, pp. 9-14.
8) Yoh, J.J. and Zhong, X.: New Hybrid Runge-Kutta Methods for Unsteady Reactive Flow Simulation, *AIAA Journal*, **42**, 2004, pp. 1593-1600.
9) Yoh, J.J.: Thermomechanical and Numerical Modeling of Energetic Materials and Multi-material Impact, Ph.D. Thesis, Theoretical and Applied Mechanics, University of Illinois of Urbana-Champaign, 2001.
10) Liu, X.-D. and Osher, S.: Convex ENO High Order Multi-dimensional Schemes without Field by Field Decomposition or Staggered Grids, *Journal of Computational Physics*, **141**, 1998, pp. 1-27.
11) Peng, D., Merriman, B., Osher, S. Zhao, H., and Kang, M.: A PDE-based Fast Local Level Set Method, *Journal of Computational Physics*, **155**, 1999, pp. 410-438.
12) Fedkiw, Marquina, A., and Merriman, B.: An Isobaric Fix for the Overheating Problem in Multimaterial Compressible Flow, *Journal of Computational Physics*, **148**, 1999, pp. 545-578.
13) Yoh, J.J., McClelland, M.A., Maienschein, J.L., Wardell, J.F., and Tarver, C.M.: Simulating Thermal Explosion of RDX-based Explosives: Model Comparison with Experiment, *Journal of Applied Physics*, **97**, 2005, 083504.
14) Yoh, J.J., McClelland, M.A., Maienschein, J.L., Nichols, A.L., and Tarver, C.M.: Simulating Thermal Explosion of HMX-based Explosives: Model Comparison with Experiment, *Journal of Applied Physics*, **100**, 2006, 073515.
15) Lee, E.L. and Tarver, C.M.: Phenomenological Model of Shock Initiation in Heterogeneous Explosives, *Physics of Fluids*, **23**, 1980, pp. 2362-2372.
16) Souers, P.C., Anderson, S., Mercer, J., McGuire, E., and Vitello, P.: JWL++: A simple Reactive Flow Code Package for Detonation, *Propellants, Explosives, Pyrotechnics*, **25**, 2000, pp. 54-58.
17) Yoh, J.J. and Kim, K.H.: Shock Compression of Condensed Matter using Eulerian Multi-material Method: Applications, *Journal of Applied Physics*, sumitted, 2007, MS #JR07-4105.